IEEE Access
Multidisciplinary ⋮ Rapid Review ⋮ Open Access Journal

Received January 7, 2021, accepted January 17, 2021, date of publication January 22, 2021, date of current version February 1, 2021.

Digital Object Identifier 10.1109/ACCESS.2021.3053861

Prediction Model for Advanced Detection of Water-Rich Faults Using 3D Anisotropic Resistivity Modeling and Monte Carlo Methods

DAIMING HU[1,2,5], XIAODONG YANG[1,2,3], MINGXIN YUE[1,2,3], YONG LI[2], AND XIAOPING WU[1,4,5]

[1]Department of Earth and Space Sciences, University of Science and Technology of China, Hefei 230026, China
[2]Key Laboratory of Geophysical Electromagnetic Probing Technologies of Ministry of Natural Resources, Institute of Geophysical and Geochemical Exploration, CAGS, Langfang 065000, China
[3]Anhui Jiaohui Technology Company Ltd., Hefei 230040, China
[4]National Geophysical Observatory at Mengcheng, Mengcheng 233500, China
[5]CAS Center for Excellence in Comparative Planetology, University of Science and Technology of China, Hefei 230026, China

Corresponding author: Xiaoping Wu (wxp@ustc.edu.cn)

This work was supported in part by the National Natural Science Foundation of China under Grant 41674076, Grant 41874084, and Grant U2039206; in part by the National Key Research and Development Program of China under Grant 2018YFE0208300 and Grant 2018YFC0603500; in part by the Key Laboratory of Geophysical Electromagnetic Probing Technologies of Ministry of Natural Resource under Grant KLGEPT201902; in part by the Fundamental Research Funds for the Central Universities under Grant WK2080000129; and in part by the Joint Open Fund of Mengcheng National Geophysical Observatory under Grant MENGO-202003.

ABSTRACT During tunnel excavation, water hazards in faults, especially steep water rich faults, pose a serious threat to safe construction in some complex mountains, which leads to low economic growth and development in these areas. Direct current resistivity method, which has high resolution and sensitivity to the low resistivity body is widely used to predict the water-bearing structures in the front of tunnel face. The current prediction models are based on the resistivity isotropic medium, however, the resistivity of water bearing fault is often anisotropic due to rock fracture. The prediction model neglecting the anisotropy is obviously inaccurate, which brings potential threats to safe construction. We develop a three-dimensional resistivity modeling for anisotropic media using unstructured finite element method. The algorithm is proved to be accurate by comparison of numerical results and analytical solutions for a whole-space model. Another classical anisotropic model also demonstrated the reliability of our code from a physical point of view. Then we propose a prediction equation to predict the position of a vertical fault with anisotropic resistivity in the front of tunnel face by the finite element simulations. The parallel Monte Carlo method is used to test and evaluate the quality of our prediction equation by simulations of 10000 random vertical fault models, results counted by the histogram showed 85.36% of the results are predicted within 10% of the error. Besides, 93.17% of the results are predicted within 15% of the error using the equation for random faults with 75 degree dip angle, which shows that our prediction model can effectively forecast steeply dipping water-rich faults or fracture zones.

INDEX TERMS Finite element method, Monte Carlo method, advanced detection in tunneling, steep water-bearing faults, resistivity anisotropy.

I. INTRODUCTION

In the construction of highways, high-speed railways, and coal mines, it is difficult but crucial to prevent water inrush hazards in tunnel excavations, especially with the increase of tunnel depth in mountain areas. Over the past decades, geophysical methods for tunnel prediction have been developed, including the direct current (DC) resistivity method, ground-penetrating radar (GPR), and the transient electromagnetic (TEM) method [1]–[6]. Compared with the other two methods, the detection depth of the DC resistivity method is larger than that of GPR. Besides, TEM is disturbed easily by the environmental noise of metal support in the tunnel while the DC resistivity method has better anti-interference

The associate editor coordinating the review of this manuscript and approving it for publication was Bo Pu.

ability. Due to its low cost, strong anti-interference ability, and high sensitivity for low resistivity bodies, DC resistivity method is widely used in detecting potentially disaster-producing water-bearing structures, including faults and karst cave [7]. Because of limited tunnel dimensions, the DC resistivity method generally uses a pole-dipole array to measure electric potential behind the tunnel face obtaining an apparent resistivity curve. The observed minimum value of the curve indicates that there is a low resistivity anomaly ahead and the offset of minimum point can be used to predict the distance of the low resistivity anomaly in front of the tunnel face.

In recent years, tunnel advanced prediction has been developed rapidly in a variety of ways. Elbaz *et al.* (2020) proposed a prediction model to forecast the earth pressure balance (EPB) shield performance with an improved particle swarm optimization (PSO) [8]. Gao *et al.* (2020) developed a real-time monitoring model to dynamically predict the earth's pressure by GRU neural network and genetic algorithm (GA) [9]. In this paper, we focus on the advanced detection of water-rich faults as low resisitivity anomaly in front of tunnel face using DC resistivity method. Prediction models are developed through physical experiments and numerical simulations for simple isotropic resistivity structures [10]–[13]. However, the actual underground geological structure is very complex. The anomaly presents arbitrary distribution and size, especially resistivity anisotropy exits in the media, which makes the available prediction equations very uncertain. Moreover, its accuracy and reliability are difficult to evaluate.

Real complex geological structures with bedding faces demonstrate varying degrees of anisotropy [14]. Reference [15] firstly introduced anisotropy into earth media in 1947. For the traditional surface DC resistivity method, resistivity anisotropy has been a hot issue in many geophysical exploration fields [16]–[20]. The anisotropic coefficient of resistivity usually varies from 1 to 3, and it also could be up to 3.7 or 4.5 in limestone strata [21]. Even if the anisotropic coefficient were 1.1, the effect of anisotropy could not be ignored [22]. If a medium with a relatively large anisotropic coefficient is simplified as isotropy, it could bring non-ignorable errors in predicting water-bearing structures. Unfortunately, there is no prediction model for advanced detection in tunnel considering resistivity anisotropy and including anisotropic coefficient in it.

Coal resources are widely distributed and abundant in the world, ranking first among all energy sources, which accounts for about 60% of the total reserves of various energy sources. But karst collapse pillars and water-conductive faults are well developed in these rich coal areas, and the angles of these geological structures are relatively large between 75° and 80° [23]–[25]. It is consistent with the development of regional joint angles [26]. The resistivity anisotropy of steeply dipping joint structures is very apparent. This likely be one of the main reasons for frequent water-inrush accidents in this area. Whether the water-inrush disaster in these geological structures with a large inclination will occur is a matter of great concern to the mineral government and enterprise. Therefore, it is of great significance to simulate the anisotropic water-rich fault with a large inclination for the prevention of disaster and regional economic development.

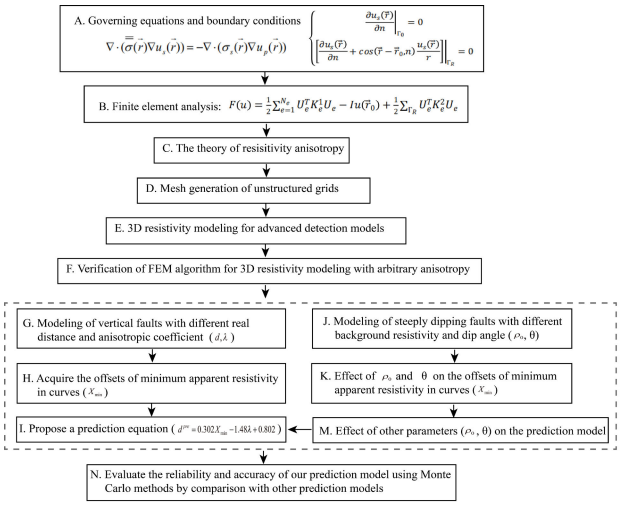

FIGURE 1. The flow chart of the overall framework idea in this article.

This study focus on the prediction model for advanced detection of steeply dipping water-bearing fault in order to effectively reduce and prevent water inrush disaster in tunneling. A three-dimensional (3D) resistivity modeling for anisotropic media using unstructured finite element (FE) method is developed, and then applied to establish a new prediction equation to predict the position of a vertical fault with anisotropic resistivity in the front of tunnel face. The effect of different parameters such as background resistivity and dip angle on the prediction model is investigated. Finally parallel Monte Carlo method is used to test and evaluate the quality of our prediction equation in comparison with available prediction models.

The content structure is organized as follows. Section II introduces governing equations, boundary conditions, and finite element analysis of the advanced detection model. We present the theory of resistivity anisotropy, unstructured grids, and calculation of pole-dipole apparent resistivity in tunnel using 3D FE resistivity modeling as well. Section III firstly verifies the effectiveness of the 3D FE modeling algorithm using two classical models, and then proposes a prediction equation for a vertical fault with anisotropic resistivity. The effect of background resistivity and dip angle on the prediction model is also discussed in this section. Section IV presents the evaluation of our prediction equation by parallel Monte Carlo method. Section V is the conclusion. Fig. 1 shows the flow chart of the overall framework idea in this study.

II. MODELLING SCHEME OF ANISOTROPIC MODEL

A. FORMULATIONS AND BOUNDARY CONDITIONS

Along with Ohm's law and the property of electric field E, which can be the gradient of potential u, the total electric

potential produced by a pole source of current strength I in an earth conductive medium can be calculated by [10]

$$\nabla \cdot \left(\overline{\overline{\sigma}}\left(\vec{r}\right) \nabla u\left(\vec{r}\right)\right) = -I\delta\left(\vec{r} - \vec{r}_0\right) \tag{1}$$

When the selected computation domain is large enough, (1) satisfies the Neumann boundary condition Γ_0 on the air-land surface and satisfies the mixed boundary condition Γ_R on the remaining boundary [27], [28]

$$\left(\partial u\left(\vec{r}\right)/\partial n\right)|_{\Gamma_0} = 0 \tag{2a}$$

$$\left[\partial u\left(\vec{r}\right)/\partial n + cos\left(\vec{r} - \vec{r}_0, n\right) \partial u\left(\vec{r}\right)/\partial r\right]\big|_{\Gamma_R} = 0 \tag{2b}$$

where $\overline{\overline{\sigma}}\left(r\right)$ represents the electric conductivity tensor, which is a third-order vector function of observation location $\vec{r}$, see detail in Section II-D. δ is the Dirac delta function, r_0 is the position of current source, and ∇ is the Laplace operator. The formulation for the total electric potential of an anisotropic medium has the same form as that of an isotropic medium.

B. FINITE ELEMENT APPROACH

To investigate 3D anisotropy resistivity modelling in tunnel prediction, with the application of Galerkin's method [29], the boundary value problem for (1) and (2) of total electric potential can be simplified as

$$F[u] = \int_{\Omega} [1/2\overline{\overline{\sigma}}(\nabla u)^2 - 2I\delta(\overrightarrow{r} - \overrightarrow{r}_0)u]d\Omega + 1/2\int_{\Gamma_R} \overline{\overline{\sigma}}(\cos(r,n)/\mathrm{r})u^2 d\Gamma \tag{3a}$$

$$\delta F\left(u\right) = 0 \tag{3b}$$

N_e is the total number of element, Ω is the target region, by unstructured meshing, equation (7) can be separated as

$$F[u] = 1/2\sum\nolimits_{e=1}^{N_e} \int_{\Omega^e} \overline{\overline{\sigma}}(\nabla u)^2 d\Omega - 2I\delta(\overrightarrow{r} - \overrightarrow{r}_0)u + 1/2\int_{\Gamma_R} \overline{\overline{\sigma}}(\cos(r,n)/\mathrm{r})u^2 d\Gamma \tag{4}$$

Ω^e is the volume unit, the potential within each element can be obtained by a linear interpolation function

$$u = U_e^T N \tag{5}$$

N is the shape function, U_e is node potential vector of the element. By substituting (5) into (4), we obtain

$$F\left(u\right) = 1/2\sum\nolimits_{e=1}^{N_e} U_e^T K_e^1 U_e - Iu\left(\vec{r}_0\right) + 1/2\sum\nolimits_{\Gamma_R} U_e^T K_e^2 U_e \tag{6}$$

K_e^1 is the volume element matrix, K_e^2 is the face element matrix. To reveal their composition, K_e^1 is shown as an example. It reads

$$K_{eij}^1 = \int_{\Omega^e} [\rho_{11}\frac{\partial N_i}{\partial x}\frac{\partial N_j}{\partial x} + \rho_{21}\frac{\partial N_i}{\partial y}\frac{\partial N_j}{\partial x} + \rho_{31}\frac{\partial N_i}{\partial z}\frac{\partial N_j}{\partial x} + \rho_{12}\frac{\partial N_i}{\partial x}\frac{\partial N_j}{\partial y} + \rho_{22}\frac{\partial N_i}{\partial y}\frac{\partial N_j}{\partial y} + \rho_{32}\frac{\partial N_i}{\partial z}\frac{\partial N_j}{\partial y} + \rho_{13}\frac{\partial N_i}{\partial x}\frac{\partial N_j}{\partial z} + \rho_{23}\frac{\partial N_i}{\partial y}\frac{\partial N_j}{\partial z} + \rho_{33}\frac{\partial N_i}{\partial z}\frac{\partial N_j}{\partial z}]dxdydz. \tag{7}$$

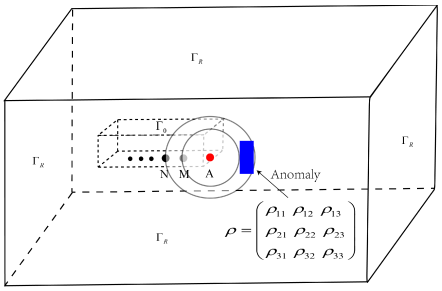

FIGURE 2. An illustration of a 3D anisotropy resistivity model of tunnel prediction. Γ_0 and Γ_R denote the air-Earth interface and the infinite domain boundary. A current source electrode A and measuring electrodes M, N are located in the tunnel. Symbol ρ is a resistivity tensor of the anomaly with symmetric.

For the isotropic medium, note that it can be simplified as $\rho_{11} = \rho_{22} = \rho_{33}$ and the other sections of the resistivity tensor are equal to zero.

By assembling all local system formulations into a single global system formulation we get

$$KU = P \tag{8}$$

$K = \sum\left(K_e^1 + K_e^2\right)$ represents the sparse and symmetric system matrix, U represents the vector of unknown potentials, and P is the source term representing the distribution of the current source.

C. SINGULARITY REMOVAL

For 3D anisotropy resistivity modelling of water-bearing anomaly structures of tunnel prediction in Fig. 2, discrete techniques often encounter singularity problems for any approximation method. It could lead to large result errors when potential electrodes are very close to the electric current source. To overcome this problem, we apply the singularity removal method by splitting the total electric potential u into primary electric potential u_p and secondary electric potential u_s. Similarly, we split the total electric conductivity σ into background electric conductivity σ_p and anomaly electric conductivity σ_s [30]

$$u = u_p + u_s \tag{9a}$$

$$\sigma = \sigma_p + \sigma_s \tag{9b}$$

The new governing equations and boundary conditions for the secondary potential u_s can be derived by substituting (9) into (1) and (2). This singularity removal was called the secondary potential approach presented by Zhao and Yedlin [31]. The boundary value problems of u_s in the anisotropic media read

$$\nabla \cdot \left(\overline{\overline{\sigma}}\left(\vec{r}\right) \nabla u_s\left(\vec{r}\right)\right) = -\nabla \cdot \left(\sigma_s\left(\vec{r}\right) \nabla u_p\left(\vec{r}\right)\right) \tag{10a}$$

$$\left(\partial u_s\left(\vec{r}\right)/\partial n\right)|_{\Gamma_0} = 0 \tag{10b}$$

$$\left[\partial u_s\left(\vec{r}\right)/\partial n + cos\left(\vec{r} - \vec{r}_0, n\right) \partial u_s\left(\vec{r}\right)/\partial r\right]\big|_{\Gamma_R} = 0 \tag{10c}$$

The finite element formulations for the boundary value problem (10a–10c) of the secondary electric potential can be derived similar to above total electric potential. Then we

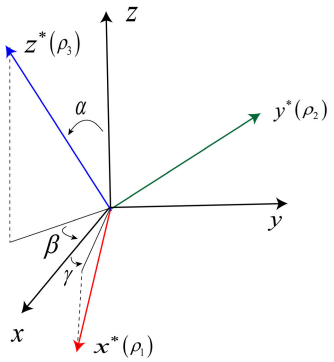

FIGURE 3. Formation of coordinate systems. The surveying coordinate system (x,y, z) can be transformed into natural rock coordinate system (x^*y^*, , z^*) by three Euler angles.

obtain the secondary electric potential u_s by 3D FE modeling, primary electric potential u_p can be analytically calculated. The total electric potential is obtained by equation (9a). The secondary field method has been proven to effectively eliminate the singularity of the source and obtain a higher accuracy [33].

D. THE THEORY OF RESISTIVITY ANISOTROPY

The 3 × 3 symmetrical anisotropic tensor of resistivity satisfies

$$\rho_{ij} = 1/\sigma_{ij} \tag{11}$$

this tensor can also be expressed as an alternative set of the six independent components by three principal resistivities ρ_1, $\rho_2\rho_3$ and three Euler angles $\alpha\beta\gamma$ [32].

$$\rho = D \begin{pmatrix} \rho_1 & 0 & 0 \\ 0 & \rho_2 & 0 \\ 0 & 0 & \rho_3 \end{pmatrix} D^T \tag{12}$$

Here

$$D = \begin{pmatrix} \cos\gamma\cos\beta & -\sin\gamma\cos\beta & \sin\beta \\ \sin\gamma\cos\alpha + \cos\gamma\sin\beta\sin\alpha & \cos\gamma\cos\alpha - \sin\gamma\sin\beta\sin\alpha & -\cos\beta\sin\alpha \\ \sin\gamma\sin\alpha - \cos\gamma\sin\beta\cos\alpha & \cos\gamma\sin\alpha + \sin\gamma\sin\beta\cos\alpha & \cos\beta\cos\alpha \end{pmatrix}$$

The rotation matrix D is related to the surveying coordinate system as shown in Fig. 3. For a layered tilted transverse isotropic medium, it includes a dip angle α and two principal resistivities, the longitudinal resistivity $\rho_L = \rho_1 = \rho_2$, which is a constant along any direction in the bedding plane, and the transverse resistivity $\rho_T = \rho_3$. We define the anisotropic coefficient as $\lambda = \sqrt{\rho}_T/\rho_L$, and the geometric mean resistivity as $\rho_M = \sqrt{\rho_L\rho_T}$. The resistivity of a TTI medium in tensor form then could be written as [33]

$$\rho = \begin{pmatrix} \rho_L & 0 & 0 \\ 0 & \rho_L cos^2\alpha + \rho_T sin^2\alpha & (\rho_L - \rho_T)\, sin\alpha cos\alpha \\ 0 & (\rho_L - \rho_T)\, sin\alpha cos\alpha & \rho_L sin^2\alpha + \rho_T cos^2\alpha \end{pmatrix} \tag{13}$$

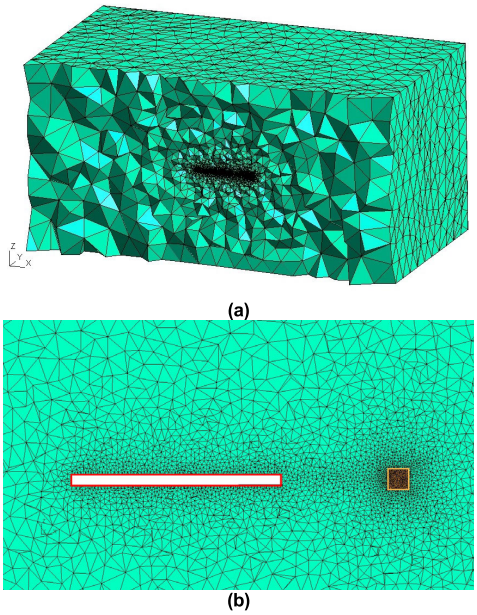

FIGURE 4. Unstructured grids of tunnel model with local refinement near the tunnel and anomaly. (a) The whole-space tunnel model. (b) The cross-section view.

E. UNSTRUCURED GRIDS

Structured tetrahedron and unstructured tetrahedron have been used in 3D electromagnetic modeling, but it was pointed out that the structured assembly of tetrahedrons gives rise to asymmetric results [33]. This factor may impede the recognition of anisotropic features from asymmetric mesh splitting in complex anisotropic models.

In our work, we mesh 3D anisotropic models with unstructured tetrahedron grids generated by an open-source software TetGen, which provides excellent adaptability for complex geometry [34]. Reference [33] has proved that the unstructured meshing technique has sufficient accuracy and computation efficiency. On the one hand, structured grids have a poor ability to meshing irregular boundaries where the elements are distorted severely. However, unstructured grids using local refinement can deal well with this problem. Also, this method in specific areas is important for achieving a balance between calculation time and solution accuracy for complicated 3D models [35]–[37]. Moreover, unstructured grids can overcome false anisotropy of 3D anisotropic resistivity modeling. These advantages provide an excellent tool to promote the development of 3D anisotropic theory in tunnel prediction. Figure 4 shows the unstructured grids of the tunnel model.

F. CALCULATION OF APPARENT RESISTIVITY

When the tunnel is deeply buried in the earth, the electric field induced by a pole current source can be approximated as a whole-space response field [13]. Thus, the electric potential has the form of

$$u = I/(4\pi\sigma r) \tag{14}$$

Because of the limited tunnel dimensions the pole–dipole configuration behind tunnel face is often used to receive the potential signal. The pole-dipole apparent resistivity ρ_s in whole-space is calculated as [10]

$$\rho_s = K^{AMN} \Delta u_{MN} / I \tag{15}$$

where

$$K^{AMN} = 4\pi AM \cdot AN / MN$$

is the array coefficient. Δu_{MN} is the potential difference of observation point M and N, which comes from 3D FE simulation above. To remove impacts of the tunnel as an empty cavity with high resistivity air, we obtain a modified apparent resistivity ρ_c by a ratio method [38]

$$\rho_c = \rho_s / c \tag{16}$$

Here

$$c = \rho_t / \rho_0$$

is the correct coefficient, ρ_0 is the resistivity of background rock, and ρ_t is the apparent resistivity of the tunnel as an only high resistivity anomaly in background rock. Thus, the modified apparent resistivity ρ_c can highlight the low resistivity anomaly in front of the tunnel face more easily such as water-bearing fault.

III. NUMERICAL TESTS AND ESTABLISHMENT OF PREDICTION MODEL

The following numerical calculations were performed on a computer with Intel(R) Xeon(R) Gold 5117 CPU @2.00GHz and 128GB RAM. To save memory and improve the calculation speed when considering the sparse property of the matrix k, the symmetric successive over relaxation (SSOR)-preconditioned conjugate gradient (PCG) method is a very efficient iterative method for solving large sparse linear equations and is used to effectively solve the Eq.(8) from the 3D anisotropic FE modeling [39]. In the first typical case of this paper with $N_e = 260,000$ total nodes, the total calculation time was within 10 seconds.

A. VERIFICATION OF FEM ALGORITHM

The accuracy of our algorithm is validated by an isotropic whole-space infinite slab model, which exists an analytical formula [40]. A schematic diagram of the model is shown in Fig. 5. The curves of electrical potential and relative error in Fig. 6 show that numerical solution can obtain high-precision with a maximum deviation of less than 0.6 percent, which indicates that this numerical method can be used for 3D resistivity modeling for whole-space tunnel prediction.

To interpret the underground anisotropic media, we present an efficient modeling algorithm that can deal with the resistivity anisotropy problem. Our numerical results of anisotropic modeling using the FE algorithm are compared with the analytical results from international publications [37], [41]. A classical anisotropic model with a Schlumberger array

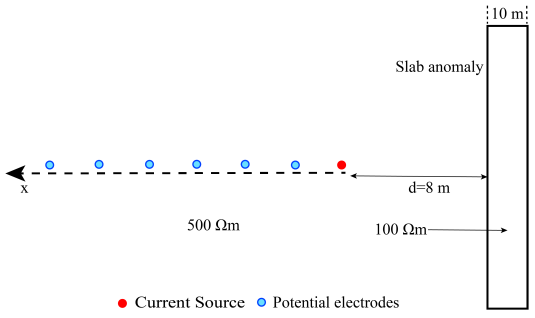

FIGURE 5. Schematic diagram of the isotropic whole-space slab model. A current source electrode is located in the origin of the x-axis, which is 8 m away from the left boundary of the slab. On the left side, 90 potential electrodes are distributed with an interval of 2 m along the x-axis.

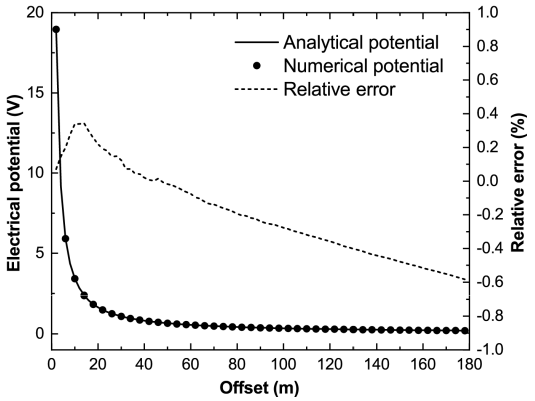

FIGURE 6. Comparison of the numerical potential by 3D FE modeling with the analytical potential.

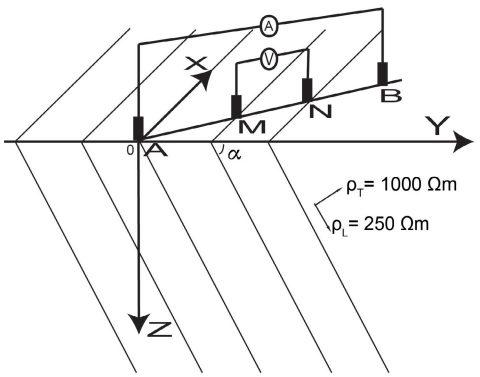

FIGURE 7. An anisotropic half-space model with a Schlumberger array. Anisotropic coefficient λ is 2.

in Fig. 7 is tested to discuss the directional variation of the apparent resistivity with changes in the dip angle of the strata. For this model, the transverse resistivity ρ_T is 1000 Ω m, the longitudinal resistivity ρ_L in the bedding plane is 250 Ω m, and the average resistivity ρ_M is 500 Ω m. The variable α represents the dip angle of the stratification. Potential and current electrodes are distributed on the surface.

Figure 8 shows a polar expression comparing our numerical results on the earth's surface for different dip angles with the theoretical results [41], which are highly consistent. For

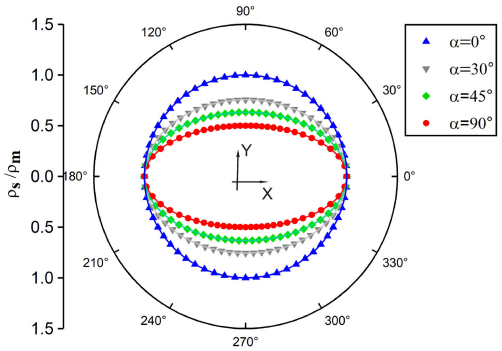

FIGURE 8. The directional variation of apparent resistivity for anisotropic model in Fig. 7 with different dip angle α.

a dip angle $\alpha = 0°$, the apparent resistivity in all directions is $\rho_s = \rho_M$. For the case of $\alpha = 90°$, the apparent resistivity along the strike direction (in the x-direction) is $\rho_s = \rho_M = 500\ \Omega$ m while the real resistivity is 250 Ω m in this direction, the apparent resistivity along the perpendicular direction to the strike is $\rho_s = \rho_L = 250\ \Omega$ m while the real resistivity is 1000 Ω m in this direction (in the y-direction). Our numerical results are in good agreement with the analytical solution. It shows a well-known anisotropy paradox [32], [42], which demonstrates the reliability of our code from a physical point of view.

B. A STEEPLY DIPPING ANISOTROPIC FAULT MODEL

Accurately forecasting steeply dipping water-rich faults or fracture zones before tunnel excavations have been an important task for government and mining enterprises, which is both a safety issue and an economic issue [43]. Considering the complex field responses for strong coupling between the anisotropic strike and slant, in spite of the effectiveness of our code for 3D complicated models with arbitrary anisotropy, here we concentrate on discussing steeply dipping fault model with anisotropy resistivity in principal directions.

Figure 9a shows a steeply dipping water-rich fault model simulated using 3D DC anisotropy resistivity modeling in this section. Figures 9b and 9c show the unstructured grids when the dip angle is $\theta = 90°$ and $\theta = 75°$, respectively. Model parameters include a 200 m × 2 m × 2 m tunnel with the transverse and longitudinal resistivity of $10^8\Omega$ m, a 10 m thickness low-resistivity slab with the geometric mean resistivity of 24 Ω m, and the background surrounding rocks with the transverse and longitudinal resistivity of 500 Ω m. The source electrode with current intensity of 1A is located in the origin of the x-axis and potential electrodes are distributed at intervals of 2 m along the x-axis behind the tunnel face.

The vertical fault models are simulated by changing the real distance ($d = 4, 6, 8, 10, 12$ m) and anisotropic coefficient ($\lambda = 1, 2, 3, 4$). The apparent resistivity profiles for the fault at $d = 4$ m, 8 m, and 12 m are shown in Fig. 10. The results at $d = 6$ m and 10 m are not shown here as they have the similar pattern. It can be seen that the offset (x_{min}) to the minimum point in apparent resistivity curves become larger with the increase of the real distance d for the same

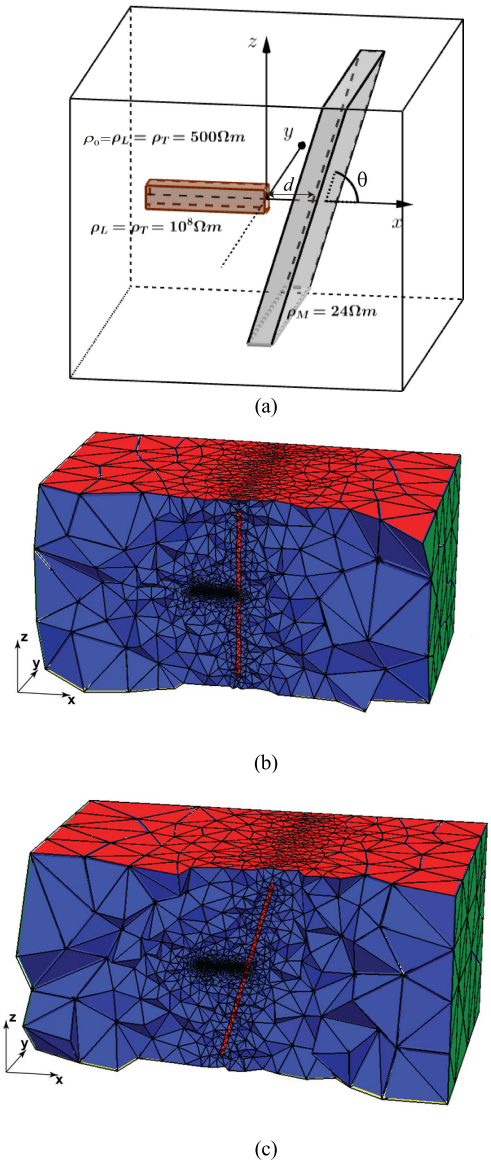

FIGURE 9. A steeply dipping anisotropic fault model in whole space. Tunnel dimensions is 200 m × 2 m × 2 m thickness of the fault is 10 m d is the real distance of fault between the tunnel face and the left boundary of the slab, θ is the dip angle of the fault. (a) Schematic diagram of geometric model. (b) Unstructured grids of a vertical fault. (c) Unstructured grids of an inclined fault with the dip angle of $\theta = 75°$.

anisotropic coefficient. The offset x_{min} is highly correlated with the real distance d and will be used for advanced prediction. Besides, the relative amplitude (the ratio of minimum apparent resistivity to background rock resistivity) decreases gradually as the real distance increases, but it is still larger than 20% at $d = 12$ m which can be observed easily.

The anisotropic coefficient shows significant impact on apparent resistivity curves. The offset increases gradually as the anisotropic coefficient rises for the fault models at the same distance, which indicates that the resistivity anisotropy should be considered for tunnel prediction. Besides, the minimum value in the apparent resistivity curve at $d = 4$ m is approximately 250Ω m ($\lambda = 3$), the relative amplitude

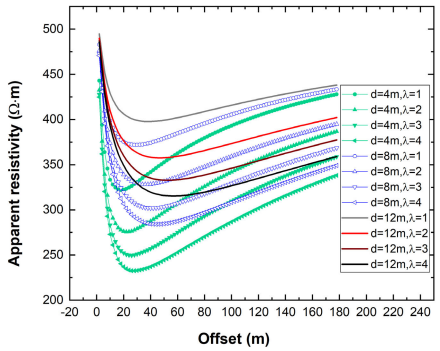

FIGURE 10. The pole-dipole apparent resistivity curves for the vertical fault at $d = 4$ m, 8 m, and 12 m and anisotropic coefficient $\lambda = 1, 2, 3, 4$.

TABLE 1. The effect of the average background resistivity (ρ_0) on the offset of minimum apparent resistivity for the anomaly with low resistivity of 20Ω m and $\lambda = 1$.

distance (m)	Background resistivity (Ωm)	Offset (m)	Minimum value (Ωm)	Abnormal amplitude
d=4	200	21	162.6	18.7%
d=4	300	21	238.6	20.4%
d=4	400	21	312.1	21.9%
d=4	500	21	389.2	22.2%
d=8	200	21	181.4	9.3%
d=8	300	21	268.8	10.4%
d=8	400	21	355.7	11.1%
d=8	500	21	442.4	11.52%

induced by anisotropic anomaly is 50% while the relative amplitude produced by an isotropic anomaly ($\lambda = 1$) at $d = 4$ m is only 36%.

The possible influence of background resistivity ρ_0 is investigated subsequently. As shown in Table 1, the offset of minimum apparent resistivity is the same regardless of the change of ρ_0 when the anisotropy coefficient and the real distance are fixed. The value of ρ_0 only affects the abnormal amplitude, and has no effect on the offset. Thus, the background resistivity is not necessary in our tunnel prediction model.

C. PROPOSED PREDICTION EQUATION

Figure 11 shows the simulation results of the above vertical fault at the distances $d = 4, 6, 8, 10, 12$ m and the anisotropic coefficient $\lambda = 1, 2, 3, 4$. The black geometric points represent the numerical results of the offset and the color lines represent the corresponding fitting curves. A prediction equation is proposed by the multiple linear regression method to predict the distance of the vertical water-rich fault as:

$$d^{\text{pre}} = f(x_{min}, \lambda) = c_1 x_{min} + c_2 + c_3 \lambda \tag{17}$$

where d^{pre} represents the prediction distance of the anomaly, x_{min} is the observed offset of the minimum apparent resistivity, regression coefficients are $c_1 = 0.302, c_2 = 0.802$ and $c_3 = -1.48$. The R-Square is a common measure of the goodness of a regression fit. The R-Square of this prediction equation is 0.976, which indicates the fit is reliable. The left two solid lines respectively represent the prediction equations

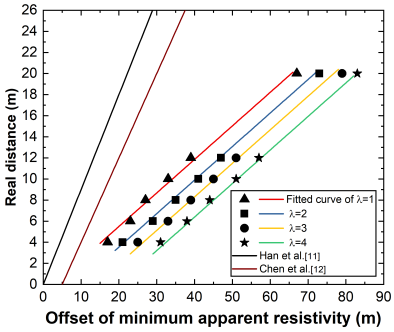

FIGURE 11. Fitted curves for the prediction model, whereas $\lambda = 1$ means the anomaly is isotropic. The black geometric points represent the numerical results of the offset and the color lines represent the corresponding fitting curves. The left two solid lines respectively represent the prediction equations proposed by other researchers.

proposed by other researchers based on physical experiment for a sphere model [11] [11] [11] and numerical simulations for isotropic model [12]. Han *et al.* [11] gave a prediction model with $c_1 = 0.80$ and $c_2 = -4.0$. Cheng *et al.* [12] suggested a prediction equation with coefficients of $c_1 = 0.90$ and $c_2 = 0.00$. Both of them did not consider the effect of resistivity anisotropy, however, even in the case of isotropy ($\lambda = 1$), their prediction error is very large. For example, the simulated offset x_{min} is 17 m for the fault model with $d = 4$ m, our prediction result is 4.4 m which is very close to the real distance. The prediction results are 9.6 m and 15.3 m for prediction models from references [11] and [12] respectively, which is much more larger than the real distance $d = 4$ m.

As for the effect of resistivity anisotropy, considering a fault model at d = 8 m with anisotropic coefficient $\lambda = 3$, the simulated offset $x_{min} = 39$ m, our prediction result is 8.1 m which is very close to the real distance. Nevertheless, the prediction result is 11.1 m while using our prediction model without resistivity anisotropy ($\lambda = 1$). It shows that the anisotropy of the resistivity has significant influence on the prediction results and should be considered. Supposing a real water-rich fault with strong resistivity anisotropy is very near the front of the tunnel face (e.g. $d = 4$ m), the prediction equations without considering resistivity anisotropy would give a very large prediction distance. The more serious the resistivity anisotropy, the greater the prediction distance, which may lead to seriously dangerous hazards and economic loss.

Moreover, the fault model at further distance is investigated. Fig. 12 shows the simulated apparent resistivity curves for a vertical fault model at the distance $d = 20$ m and $\lambda = 1, 2, 3, 4$. The observed offsets are drawn point by point in Fig. 11. It can be seen that they are very consistent with the fitting line of our prediction equation, which further proves the accuracy of our prediction model at a large distance.

IV. EVALUATION OF PREDICTION MODEL BY MONTE CARLO METHODS

Monte Carlo methods are statistical methods that use random numbers to deal with probabilistic distributions. Monte Carlo

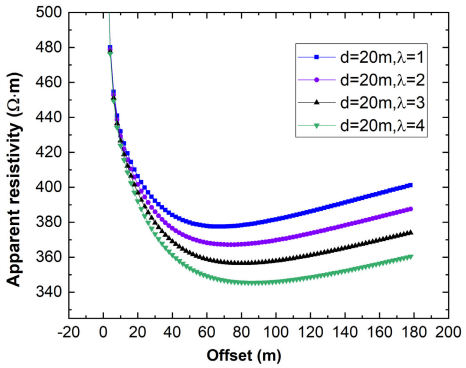

FIGURE 12. The pole-dipole apparent resistivity curves for the vertical fault at $d = 20$ m and anisotropic coefficient $\lambda = 1, 2, 3, 4$.

methods are becoming essentially practical tools for solving problems in geophysics [44], [45]. To date, practical use of Monte Carlo has become popular for time-consuming modeling through algorithms running on high-speed computers [46]–[48].

Monte Carlo methods are first used for non-deterministic problems in tunnel prediction in this study. Due to the problem of fluid connectivity, the distribution of water in the fault may be very complex, i.e., the size and shape of low resistivity anomalies in water bearing fault model are quite different, which can be simulated by randomly distributed resistivity anomaly. The Monte Carlo method is applied to the numerical simulation of tunnel advanced detection, forming a large number of random vertical fault models, in which each unstructured unit has a random low resistivity value less than the background resistivity 500Ω m, and each unit has a random anisotropic coefficient varying from 1 to 4.

For the same surveying conditions using the pole-dipole configuration, different resistivity distributions of the anomaly will lead to different prediction results. The prediction result for i^{th} random model is defined as

$$d_i^{pre} = f(\boldsymbol{\rho}_\mathbf{i}; \boldsymbol{\lambda}_\mathbf{i}) \tag{18}$$

where d_i^{pre} represents the prediction distance of the anomaly, f represents the prediction function, $\boldsymbol{\rho}_\mathbf{i}$ represents the random distribution of low resistivity structures, $\boldsymbol{\lambda}_\mathbf{i}$ represents random distribution of anisotropic coefficient. If the total number is large enough, the statistical results can simulate the probability distribution of the distances that are close to the real situation, and thus the reliability of different prediction equations can be judged quantitatively.

As all calculations are independent, parallel Monte Carlo calculations are introduced. We tested the calculation efficiency of two different Monte Carlo methods on a PC platform. The Monte Carlo methods is calculated by a symmetric successive overrelaxation pre-conditioner (SSOR-PCG), while another parallel Monte Carlo methods on the OpenMP specification is run by PARDISO solver. The running time of the SSOR-PCG method is 205s, which is approximately 9 times larger than that of the parallel method (22s). In the following, we have conducted 10000 random

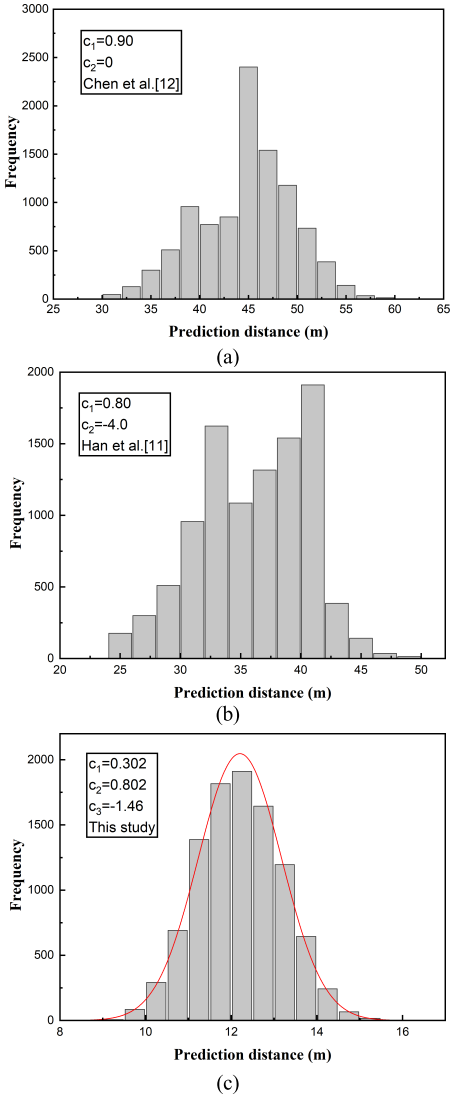

FIGURE 13. The distribution of prediction results for 10000 random vertical fault models at the real distance $d = 12$ m by the prediction equations proposed in ref. [12] (a), ref. [11] (b) and this study (c).

models using parallel Monte Carlo methods. A series of data $d_1^{pre}, d_2^{pre}, \ldots, d_i^{pre}$ are obtained to evaluate the reliability of our prediction equation. To avoid accidental errors, 1% Gaussian errors were added in the synthesized data.

Figure 13 shows prediction results from different prediction equations for 10000 random vertical fault models at the real distance $d = 12$ m. The predicted distances by Cheng *et al.* [12] range from 30 m to 60 m (Figure 13a), which are far from the true distance of anomaly. Figure (13b) shows that predicted distances by Han *et al.* [11] range from 24 m to 50 m, which are more than twice the real distance of the anomaly. The two prediction results greatly exaggerate the distance of water bearing fault in front of the tunnel face, which will lead to serious danger in the process of actual tunnel excavation. Figure (13c) shows that most of the prediction distances simulated by our proposed prediction equation are very close to the real distance of 12 m with a relatively narrow range and accord with the normal distribution

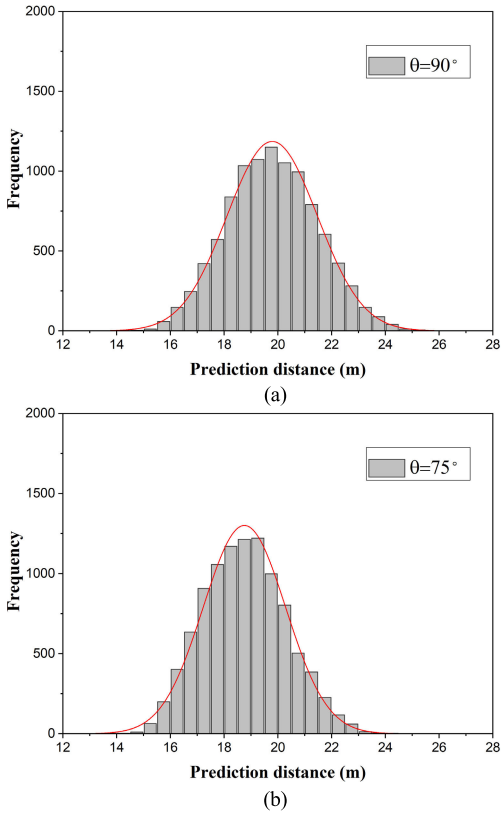

FIGURE 14. The distribution of prediction results for 10000 random fault models with anisotropy at the real distance d = 20 m by our prediction equation. (a) random vertical faults, (b) random steeply dipping faults with $\theta = 75°$.

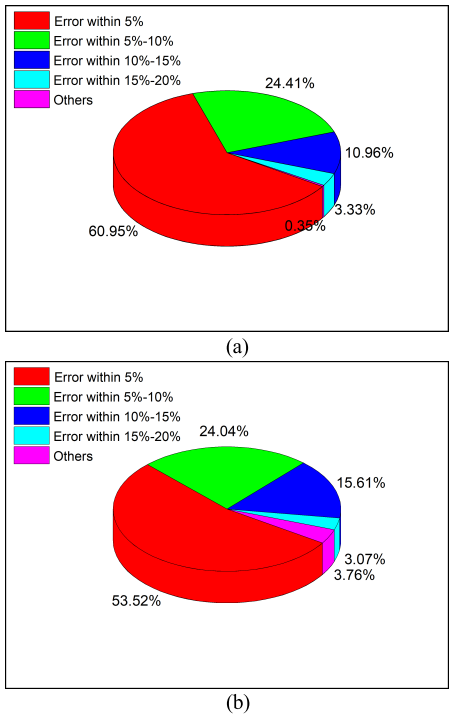

FIGURE 15. Pie chart of prediction error distribution for two fault models (a) random vertical faults, (b) random steeply dipping faults with $\theta = 75°$.

of probability perfectly, which demonstrates our prediction model is accurate and reliable.

Because the fault dip angle changes, the unstructured mesh needs to be redivided in 3D resistivity FE modeling, so the dip angle cannot be changed randomly in Monte Carlo method. We focus on advanced detection of steeply dipping water-bearing fault using the prediction equation (17) from the simulations for a vertical fault, the effect of the dip angle on our prediction should be considered. Then 10000 random models for a vertical fault ($\theta = 90°$) and a steeply dipping fault ($\theta = 75°$) at the real distance $d = 20$m are simulated using parallel Monte Carlo methods, respectively. The predicted results by prediction equation (17) are shown in Fig. 14.

The prediction results for vertical fault $\theta = 90°$ are shown in Fig. 14a, the maximum probability distribution locates at the real distance of 20 m with a relatively narrow range and accord with the normal distribution of probability perfectly. As for the prediction results for steeply dipping fault $\theta = 75°$ shown in Fig. 14b, the prediction distance of the maximum probability is approximately 19 m only with the error of 5%, the normal distribution of probability also works well. Fig. 15 presents the statistical results in detail. 60.95% of the results are predicted within 5% of the error, and 85.36% of the results are predicted within 10% of the error for random vertical fault models (Fig. 15a). As for statistical results of random steeply dipping fault models (Fig. 15b), 53.52% of the results are predicted within 5% of the error and moreover 93.17% of the results are predicted within 15% of the error using the prediction equation (17). These results prove that our prediction model is reliable and sufficiently accurate in predicting the distance of steep dip fault in front of the tunnel face. Meanwhile, the application of the random fault model in the Monte Carlo method also makes our prediction conditions closer to the real situation of tunnel advanced detection.

V. CONCLUSION

In the process of actual tunnel excavation, the fault in front of the tunnel face is very complex, but the water damage is mostly caused by steep water bearing fault. Due to the problem of water connectivity, the fluid distribution in water bearing fault can be arbitrary, and its resistivity distribution is arbitrary and anisotropic owing to the direction of fractures. A 3D resistivity modeling for anisotropic media using unstructured finite element method is developed in this paper. On this base, a prediction equation to predict the position of a vertical fault with anisotropic resistivity in the front of tunnel face is proposed for the first time. The parallel Monte Carlo method is used to test and evaluate the quality of our prediction equation by simulations of 10000 random vertical fault models, statistics show 85.36% of the results are predicted within 10% of the error. The results show that our prediction results are much better than the existing prediction models. The influence of steep dip angle of fault is small and acceptable, 93.17% of the results are predicted within 15% of the error using the equation for random faults with 75 degree dip angle, which shows that our prediction model is

reliable and accurate in predicting the distance of steep dip fault in front of the tunnel face. Moreover, The Monte Carlo method provides a new way for quantitative description of accuracy and reliability of advance detection in tunnel. Prediction of time-dependent groundwater inflow into a tunnel is very important [49], its dynamic monitoring using our DC resistivity method is the focus of future research.

REFERENCES

[1] J. Cheng, F. Li, S. Peng, X. Sun, J. Zheng, and J. Jia, "Joint inversion of TEM and DC in roadway advanced detection based on particle swarm optimization," *J. Appl. Geophys.*, vol. 123, pp. 30–35, Dec. 2015.
[2] J. Yu, R. Malekian, J. Chang, and B. Su, "Modeling of whole-space transient electromagnetic responses based on FDTD and its application in the mining industry," *IEEE Trans. Ind. Informat.*, vol. 13, no. 6, pp. 2974–2982, Dec. 2017.
[3] Z. Jiang, S. Liu, and R. Malekian, "Analysis of a whole-space transient electromagnetic field in 2.5-dimensional FDTD geoelectric modeling," *IEEE Access*, vol. 5, pp. 18707–18714, 2017.
[4] J. Li and Z.-L. Wang, "The application of tunnel reflection tomography in tunnel geological advanced prediction based on regression analysis," *Open Civil Eng. J.*, vol. 9, no. 1, pp. 805–810, Oct. 2015.
[5] J. Martines-López, J. Rey, J. Dueñas, C. Hidalgo, and J. Benavente, "Electrical tomography applied to the detection of subsurface cavities," *J. Cave Karst Stud.*, vol. 75, no. 1, pp. 28–37, Apr. 2013.
[6] P. Martínez-Pagán, D. Gómez-Ortiz, T. Martín-Crespo, J. I. Manteca, and M. Rosique, "The electrical resistivity tomography method in the detection of shallow mining cavities. A case study on the Victoria Cave, Cartagena (SE Spain)," *Eng. Geol.*, vol. 156, no. 9, pp. 1–10, Apr. 2013.
[7] S. Li, B. Liu, L. Nie, Z. Liu, M. Tian, S. Wang, M. Su, and Q. Guo, "Detecting and monitoring of water inrush in tunnels and coal mines using direct current resistivity method: A review," *J. Rock Mech. Geotech. Eng.*, vol. 7, no. 4, pp. 469–478, Aug. 2015.
[8] K. Elbaz, S.-L. Shen, W.-J. Sun, Z.-Y. Yin, and A. Zhou, "Prediction model of shield performance during tunneling via incorporating improved particle swarm optimization into ANFIS," *IEEE Access*, vol. 8, pp. 39659–39671, 2020.
[9] M.-Y. Gao, N. Zhang, S.-L. Shen, and A. Zhou, "Real-time dynamic Earth-pressure regulation model for shield tunneling by integrating GRU deep learning method with GA optimization," *IEEE Access*, vol. 8, pp. 64310–64323, 2020.
[10] Y. Liu and X. Wu, "Parallel Monte Carlo method for advanced detection in tunnel incorporating anisotropic resistivity effect," (in Chinese), *Chin. J. Geophys.*, vol. 59, no. 11, pp. 4297–4309, 2016.
[11] G. Han, D. Zhuang, J. Tian, and M. Wu, "Primary theory on the mine direct current method to pilot predict sphere structure and study on san trough simulation experiment," (in Chinese), *Coal Eng.*, vol. 3, no. 12, pp. 69–72, 2009.
[12] J. Cheng, Y. Wang, S. Yu, and D. Li, "The principle and application of advance surveying in roadway excavation by resistivity method," (in Chinese), *Coal Geol. Explor.*, vol. 28, no. 4, pp. 60–62, 2000.
[13] J.-G. Huang, J.-L. Wang, and B.-Y. Ruan, "Anomalous of large polar distance dipole-dipole resistivity sounding in tunnel," (in Chinese), *Prog. Geophys.*, vol. 6, no. 22, pp. 1935–1941, 2007.
[14] P. Jaysaval, D. V. Shantsev, S. de la Kethulle de Ryhove, and T. Bratteland, "Fully anisotropic 3-D EM modelling on a Lebedev grid with a multigrid pre-conditioner," *Geophys. J. Int.*, vol. 207, no. 3, pp. 1554–1572, Dec. 2016.
[15] R. Maillet, "The fundamental equations of electrical prospecting," *Geophysics*, vol. 12, no. 4, pp. 529–556, Oct. 1947.
[16] C. Yin and P. Weidelt, "Geoelectrical fields in a layered earth with arbitrary anisotropy," *Geophysics*, vol. 64, no. 2, pp. 426–434, Mar. 1999.
[17] C. C. Pain, J. V. Herwanger, J. H. Saunders, M. H. Worthington, and C. R. de Oliveira, "Anisotropic resistivity inversion," *Inverse Problems*, vol. 19, no. 5, p. 1081, 2003.
[18] Y. Li and K. Spitzer, "Finite element resistivity modelling for three-dimensional structures with arbitrary anisotropy," *Phys. Earth Planet. Interiors*, vol. 150, nos. 1–3, pp. 15–27, May 2005.
[19] J.-H. Kim, M.-J. Yi, S.-J. Cho, J.-S. Son, and W.-K. Song, "Anisotropic crosshole resistivity tomography for ground safety analysis of a high-storied building over an abandoned mine," *J. Environ. Eng. Geophys.*, vol. 11, no. 4, pp. 225–235, Dec. 2006.
[20] B. Zhou, M. Greenhalgh, and S. A. Greenhalgh, "2.5-D/3-D resistivity modelling in anisotropic media using Gaussian quadrature grids," *Geophys. J. Int.*, vol. 176, no. 1, pp. 63–80, Jan. 2009.
[21] N. Linde and L. B. Pedersen, "Evidence of electrical anisotropy in limestone formations using the RMT technique," *Geophysics*, vol. 69, no. 4, pp. 909–916, Jul. 2004.
[22] T. Wiese, S. Greenhalgh, and L. Marescot, "DC resistivity sensitivity patterns for tilted transversely isotropic media," *Near Surf. Geophys.*, vol. 7, no. 2, pp. 125–139, 2009.
[23] Y. Liu, "Analysis of rationally setting water-proof coal pillar for water-conductive fault in deep mining area," (in Chinese), *Coal Mining Technol.*, vol. 13, no. 1, pp. 21–22, 2008.
[24] J. Wu, "Analysis of rationally setting water-proof pillar for fault of water-rich Laneway in Baixiangshan iron mine," (in Chinese), *Modern Mining*, vol. 1, no. 1, pp. 15–18, 2011.
[25] H. Bai, X. Mao, W. U. Yu, and Z. Chen, "Research on water-reserved mining with high water pressure under large-scale thrust-fault in Ordovician Karst," (in Chinese), *Chinese J. Rock Mech. Eng.*, vol. 28, no. 2, pp. 246–252, 2009.
[26] H. Si, W. Yang, and W. Wu, "The grown-up conditions and water-conducting behavior of karstic collapse pillor," (in Chinese), *Coal Eng.*, vol. 10, no. 4, pp. 52–55, 2004.
[27] Z. Bing and S. A. Greenhalgh, "Finite element three-dimensional direct current resistivity modelling: Accuracy and efficiency considerations," *Geophys. J. Int.*, vol. 145, no. 3, pp. 679–688, Jun. 2001.
[28] T. Günther, C. Rücker, and K. Spitzer, "Three-dimensional modelling and inversion of DC resistivity data incorporating topography–II. Inversion," *Geophys. J. Int.*, vol. 166, no. 2, pp. 506–517, Aug. 2006.
[29] P. G. Ciarlet, "The finite element method for elliptic problems," *Classics Appl. Math.*, vol. 40, pp. 1–511, Jan. 2002.
[30] Y. Li and K. Spitzer, "Three-dimensional DC resistivity forward modelling using finite elements in comparison with finite-difference solutions," *Geophys. J. Int.*, vol. 151, no. 3, pp. 924–934, Dec. 2002.
[31] S. Zhao and M. J. Yedlin, "Some refinements on the finite-difference method for 3-D DC resistivity modeling," *Geophysics*, vol. 61, no. 5, pp. 1301–1307, Sep. 1996.
[32] C. Yin, "Geoelectrical inversion for a one-dimensional anisotropic model and inherent non-uniqueness," *Geophys. J. Int.*, vol. 140, no. 1, pp. 11–23, Jan. 2000.
[33] W. Wang, X. Wu, and K. Spitzer, "Three-dimensional DC anisotropic resistivity modelling using finite elements on unstructured grids," *Geophys. J. Int.*, vol. 193, no. 2, pp. 734–746, May 2013.
[34] H. Si and A. TetGen, "A quality tetrahedral mesh generator and three-dimensional delaunay triangulator," Weierstrass Inst. Appl. Anal. Stochastic, Berlin, Germany, Tech. Rep. 81, Jan. 2006.
[35] A. Franke, R.-U. Börner, and K. Spitzer, "Adaptive unstructured grid finite element simulation of two-dimensional magnetotelluric fields for arbitrary surface and seafloor topography," *Geophys. J. Int.*, vol. 171, no. 1, pp. 71–86, Oct. 2007.
[36] Z. Ren and J. Tang, "3D direct current resistivity modeling with unstructured mesh by adaptive finite-element method," *Geophysics*, vol. 75, no. 1, pp. H7–H17, Jan. 2010.
[37] Z. Ren, L. Qiu, J. Tang, X. Wu, X. Xiao, and Z. Zhou, "3-D direct current resistivity anisotropic modelling by goal-oriented adaptive finite element methods," *Geophys. J. Int.*, vol. 212, no. 1, pp. 76–87, Jan. 2018.
[38] B. Liu, S.-C. Li, S.-C. Li, and S.-H. Zhong, "Study of advanced detection of water-bearing geological structures with DC resistivity method," (in Chinese), *Rock Soil Mech.*, vol. 30, no. 10, pp. 3094–3100, 2009.
[39] X. Wu, "A 3-D finite-element algorithm for DC resistivity modelling using the shifted incomplete Cholesky conjugate gradient method," *Geophys. J. Int.*, vol. 154, no. 3, pp. 947–956, Sep. 2003.
[40] J. G. Huang, J.-L. Wang, and B. Y. Ruan, "A study on advanced detection using DC resistivity method in tunnel," (in Chinese), *Chin. J. Geophys.*, vol. 49, no. 5, pp. 1529–1538, 2006.
[41] D. S. Parasnis, *Principles of Applied Geophysics*, 3rd ed. London, U.K.: Chapman & Hall, 1986.
[42] K. A. Watson and R. D. Barker, "Differentiating anisotropy and lateral effects using azimuthal resistivity offset Wenner soundings," *Geophysics*, vol. 64, no. 3, pp. 739–745, May 1999.
[43] G. Q. Xue, Y. J. Yan, X. Li, and Q. Y. Di, "Transient electromagnetic S-inversion in tunnel prediction," *Geophys. Res. Lett.*, vol. 34, no. 18, pp. 529–538, 2007.

[44] K. Gallagher, K. Charvin, S. Nielsen, M. Sambridge, and J. Stephenson, "Markov chain Monte Carlo (MCMC) sampling methods to determine optimal models, model resolution and model choice for earth science problems," *Mar. Petroleum Geol.*, vol. 26, no. 4, pp. 525–535, Apr. 2009.
[45] N. Piana Agostinetti, G. Giacomuzzi, and A. Malinverno, "Local three-dimensional earthquake tomography by trans-dimensional Monte Carlo sampling," *Geophys. J. Int.*, vol. 201, no. 3, pp. 1598–1617, Jun. 2015.
[46] K. Mosegaard and M. Sambridge, "Monte Carlo analysis of inverse problems," *Inverse Problems*, vol. 18, no. 3, pp. R29–R54, Jun. 2002.
[47] S.-S. Lin, S.-L. Shen, A. Zhou, and Y.-S. Xu, "Approach based on TOPSIS and Monte Carlo simulation methods to evaluate lake eutrophication levels," *Water Res.*, vol. 187, Dec. 2020, Art. no. 116437.
[48] A. Seifi, M. Dehghani, and V. P. Singh, "Uncertainty analysis of water quality index (WQI) for groundwater quality evaluation: Application of monte-carlo method for weight allocation," *Ecol. Indicators*, vol. 117, Oct. 2020, Art. no. 106653.
[49] X.-X. Liu, S.-L. Shen, Y.-S. Xu, and Z.-Y. Yin, "Analytical approach for time-dependent groundwater inflow into shield tunnel face in confined aquifer," *Int. J. Numer. Anal. Methods Geomech.*, vol. 42, no. 4, pp. 655–673, Mar. 2018.

DAIMING HU is currently pursuing the Ph.D. degree with the School of Earth and Space Sciences, University of Science and Technology of China (USTC). He has applied for invention patents and published several articles. His research interests include the electromagnetic prospecting method and anisotropic theory. Especially, he is good at numerical simulation of transient electromagnetic method (TEM) and advanced detection of dc resistivity method. He was awarded a scholarship sponsored by the China Scholarship Council to study at the University of Cologne, Germany, in 2020.

XIAODONG YANG is currently pursuing the Ph.D. degree with the School of Earth and Space Sciences, University of Science and Technology of China. His research interest includes the modeling and inversion of time-domain controlled-source electromagnetic method and its applications.

MINGXIN YUE is currently a Postdoctoral Research Fellow with the University of Science and Technology of China. His research interest includes 3D imaging of electromagnetic data.

YONG LI is currently a Researcher with the Key Laboratory of Geophysical Electromagnetic Probing Technologies of Ministry of Natural Resources of China. His research interest includes applied geophysics.

XIAOPING WU received the B.Sc. degree in geophysics from Jilin University, in 1988, the master's degree from the China University of Geosciences, Beijing, in 1993, and the Ph.D. degree in geophysics from USTC, in 1998. He is currently a Professor with the University of Science and Technology of China (USTC). He conducted a cooperative research at TU Freiberg University, Germany, in 2003. He has published more than 30 peer-reviewed articles in *Journal of Geophysical Research*, *Geophysical Journal International*, *Applied Physics Letters*, *Physical Review B*, and so on. He is currently the Director of geophysics with the University of Science and Technology of China. His research interest includes the modeling and inversion theory of electromagnetic methods in geophysics. He is also a member of the Geomagnetic Committee of the Chinese Geophysical Society.